In-vivo Validation of a Novel Robotic Platform for Endovascular Intervention

Giulio Dagnino, Dennis Kundrat, Trevor M. Y. Kwok, Mohamed E. M. K. Abdelaziz, Wenqiang Chi, Anh Nguyen, Celia Riga, Guang-Zhong Yang

***Abstract*— *Objective:* In-vivo validation on animal setting of a pneumatically propelled robot for endovascular intervention, to determine safety and clinical advantage of robotic cannulations compared to manual operation. *Methods:* Robotic assistance and image-guided intervention are increasingly used for improving endovascular procedures with enhanced navigation dexterity and accuracy. However, most platforms developed in the past decade still present inherent limitations in terms of altered clinical workflow, counterintuitive human-robot interaction, and a lack of versatility. We have created a versatile, highly integrated platform for robot-assisted endovascular intervention aimed at addressing such limitations, and here we demonstrate its clinical usability through in-vivo animal trials. A detailed in-vivo study on four porcine models conducted with our robotic platform is reported, involving cannulation and balloon angioplasty of five target arteries. *Results:* The trials showed a 100% success rate, and post-mortem histopathological assessment demonstrated a reduction in the incidence and severity of vessel trauma with robotic navigation versus manual manipulation. *Conclusion:* In-vivo experiments demonstrated that the applicability of our robotic system within the context of this study was well tolerated, with good feasibility, and low risk profile. Comparable results were observed with robotics and manual cannulation, with clinical outcome potentially in favor of robotics. *Significance:* This study showed that the proposed robotic platform can potentially improve the execution of endovascular procedures, paving the way for clinical translation.**

***Index Terms*—Endovascular robotics, In-vivo animal study, Teleoperation.**

I. Introduction

SURGICAL robotics is one of the fastest growing sectors in medicine, which in the last 30 years has evolved to become a major area of innovation [1]. Robotic platforms are currently used in clinical applications including neurosurgery [2], orthopedics [3], [4], ear-nose-throat [5], [6], laparoscopy [7], and endoluminal procedures [8].

Endovascular interventions are surgical procedures that can benefit from the application of robotic assistance [9]. Endovascular techniques are widely used for the treatment of cardiovascular disease – the most common cause of death in the world [10]. Catheters and guidewires are used to perform various tasks by navigating the vasculature to reach the desired anatomical target. Examples of endovascular procedures include *stenting* [11], *cardiac ablation* [12], *embolization* [13], and *device delivery* [14]. Vascular navigation is challenging and requires excellent endovascular skills to avoid unintentional (yet frequent) contacts between the manipulated instruments and the vessel walls, with potential for perforation and injuries [15]. Thus far, there are increasing interests in robotic technology to accurately maneuver catheters and guidewires. Benefits include improved stability and precision, easier access to difficult-to-reach anatomy, reduced radiation doses, and improved patient comfort [1]. Several endovascular robotic platforms have been developed, proposing different solutions such as tendon-driven, electromagnetic, and hydraulic drives. Readers are referred to references [1], [9], [10] for detailed reviews of the state of the art.

Despite increased use of robotic platforms for endovascular intervention, most existing systems tend to have a number of limitations regarding clinical usability [9], which can be grouped into four categories.

1) *Low integration levels within clinical workflow:* Robotic navigation is often limited to a defined part of the endovascular procedure with limited collaborative instrument handling.
2) *Counterintuitive design of Human-Machine Interfaces:* Commercial systems rarely imitate the human motion patterns of the procedure, e.g., relies on joysticks, thus limiting the operator's endovascular skills.
3) *Limited Guidance:* Endovascular operators strongly rely on both haptic and visual guidance during manual procedures. Many commercial robotic systems lack of haptic feedback, and the vessel/instrument contact forces are not transmitted to the operator [15]. In terms of visual guidance, navigation still relies on 2D fluoroscopy [10], which exposes both the patient and (partially) the operator

Giulio Dagnino and Dennis Kundrat were with the Hamlyn Centre for Robotic Surgery, Imperial College London, U.K. They are now with the University of Twente, The Netherlands. *(Giulio Dagnino and Dennis Kundrat contributed equally to this work.) (Corresponding author: Giulio Dagnino, email: g.dagnino@utwente.nl).*

Trevor M. Y. Kwok and Celia Riga are with the Faculty of Medicine, Department of Surgery and Cancer, Imperial College London, U.K.

Mohamed E. M. K. Abdelaziz and Wenqiang Chi are with the Hamlyn Centre for Robotic Surgery, Imperial College London, U.K.

Anh Nguyen was with the Hamlyn Centre for Robotic Surgery, Imperial College London, U.K. He is now with the University of Liverpool, U.K.

Guang-Zhong Yang is with the Institute of Medical Robotics, Shanghai, Jiao Tong University, China.

This research was funded by the UK EPSRC (EP/N024877/1).

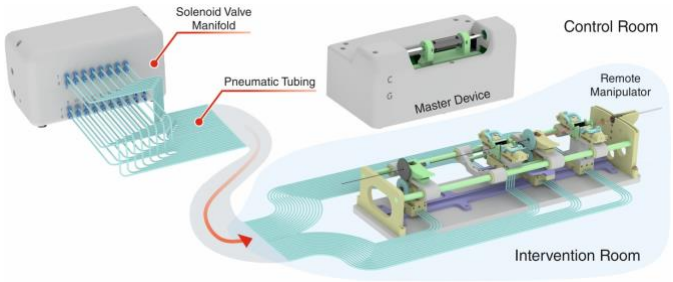

Fig. 1. Key components of the robotic platform: master device, MR-safe remote manipulator, and valve manifold for pneumatic actuation.

to ionizing radiation.

4) *Limited versatility:* Most commercial systems use manufacturer-specific instruments, which can affect the general applicability and versatility of the platforms [16] and are expensive.

Research conducted herein is aimed at addressing the aforementioned limitations. In previous studies [15]–[18] we have created a versatile, highly integrated platform for robot-assisted endovascular intervention. The robotic platform, named as CathBot (Fig. 1), has the following features: *1)* small footprint and intuitive control enabling optimal cooperation with the operator and integration with the clinical workflow; *2)* user-friendly, ergonomic master manipulator that replicates the endovascular maneuver patterns; *3)* enhanced navigation, including haptic and visual (fluoroscopy, magnetic resonance imaging (MRI)) guidance; *4)* enhanced versatility with potential application to an extended range of endovascular procedures.

In preparation of the in-vivo animal trials here reported, seven expert vascular surgeons have tested CathBot in a clinically realistic in-vitro environment under fluoroscopy. Readers are referred to [19].

The current study aims at assessing the performance, feasibility, and safety of our robotic platform through different in-vivo endovascular procedures on porcine models. The detailed in-vivo animal study reported shows that our platform would be able to resolve challenges of precise endovascular robotic navigation, surgical workflow integration, and safety.

II. Robotic Platform

This section provides an overview of our robotic platform. These concepts have been applied by our group in prior studies [16], [19], [20] – which we refer the readers to for a detailed analysis – and are summarized here (along with the Supplemental Materials) for completeness of this work.

The robotic platform (Fig. 1) comprises a master device for teleoperation and user interface, a remotely operated manipulator directly attachable to the surgical table for remote manipulation of endovascular instrumentation, and a navigation system that interfaces preceding devices with the real-time imaging system (e.g., fluoroscopy).

The master device mimics the handling of guidewires and catheters, i.e., grasping, push/pull or rotary motion. It further enables rotary and linear user input with force/torque feedback based on linear and rotary motors. After linear displacement of the user handle to advance or retract the selected instrument, the integrated linear motor homes the handle automatically. Hence, mimicking the human motion pattern, arbitrary strokes can be commanded.

The remote manipulator replicates the users' motion commands captured by the master manipulator. Translation and rotation of the actual catheter and guidewire are achieved via linear and rotary drivers. Customized pneumatic clamps are designed to transmit forces to both instruments in the translation phase. The remote manipulator comprises two plug-and-play mechanisms (one for catheter, one for guidewire) for docking and quick-exchange of vascular instruments. All remote components are MR-compatible, for potential future use with MRI. The remote manipulator is placed close to the patient in the interventional room while the master device is in the control room together with the navigation system and a valve manifold that controls the pneumatic motors. The operator interacts with the master device from the control room while watching at the real-time video stream provided by the imaging system and displayed in the navigation system (Fig. 2A). In addition to providing visual guidance, the navigation system processes the video stream generating dynamic virtual fixtures to constraint the instrument motion and guide the operator through the vasculature. This haptic guidance, rendered through the master device and perceived as a friction, is calculated by tracking in real-time the relative position of the instrument and the vessel walls: the closer the instrument is to the vessel wall, the higher is the friction perceived by the user in the master device. Moreover, the velocity of the remote manipulator is slowed down accordingly (more details in [16], [19], [20] and in the Supplemental Materials). The goal is avoiding potentially harmful peak-force impacts between the instruments and the vessel walls. Finally, the system processes the operator's inputs and generates motion commands for the remote manipulator to navigate the surgical instruments (either catheter or guidewire) through the vasculature. Standard commercially available catheters and guidewires can be easily connected to and manipulated by the remote manipulator, and when required by the clinical application, can be quickly exchanged by the surgeon's assistant in few seconds. It's worth noting that only the remote manipulator is in the interventional room, while the rest of the platform (master device, navigation system and additional electronics) are in the control room. This has the advantages of protecting the first operator from x-ray exposure, while minimizing the impact of the platform on the clinical workflow facilitating the cooperation with the clinical team.

III. In-Vivo Animal Study

Pilot validation studies were conducted in four *in-vivo* porcine models (Fig. 2) to demonstrate the feasibility of our robotic platform assessing its safety and clinical usability by comparison with standard manual procedures. An experienced senior vascular surgeon with previous experience with the robotic platform (> 40 h) conducted robotic ($R=2$) and manual reference ($M=2$) studies. In each animal model, four surgical tasks were executed under general anesthesia targeting the following arteries: *(i)* left common iliac artery (LCIA, Fig. 2E

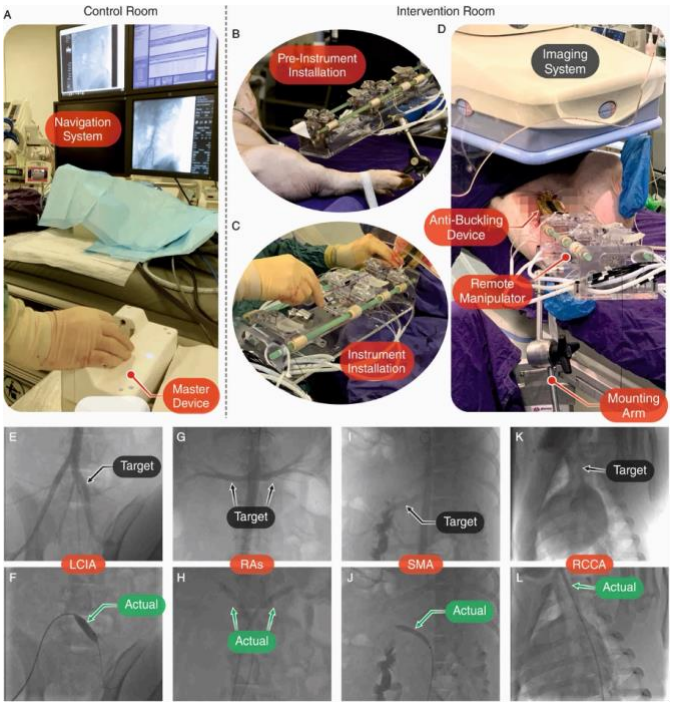

Fig. 2. In-vivo evaluation. (A) The clinician completes the procedure from the control room using the master device guided by the navigation system. (B, D) The remote manipulator is connected to the mounting arm and positioned close to the animal. (C) Manual instrument replacement on remote robot. (D) Anti-buckling device connects robot and introducer. (E-L) Exemplary fluoroscopy images of targeted arteries: target cannulation points are indicated by black arrows (E, G, I, K); green arrows show the actual catheterization points (F, H, J, L) where angioplasty balloons were inflated (darker grey shadows). The image showing the actual catheterization of RAs (G, H) is composed by two fluoroscopy images overlayed for convenience (one showing the cannulation of LRA and one RRA).

and 2F); *(ii)* left and right renal arteries (LRA, RRA, Fig. 2G and 2H); *(iii)* superior mesenteric artery (SMA, Fig. 2I and 2J); and *(iv)* right common carotid artery (RCCA, Fig. 2K and 2L). The vascular targets were selected according to common clinical indications for balloon angioplasty and complexity levels of the associated workflow. For example, instrument navigation and manipulation in cannulation of renal/mesenteric arteries differ from iliac arteries due to branch angles and tortuosity. Examples are shown in the Supplemental Video.

Following selective non-subtracted angiograms (Fig. 2E to 2L), the aforementioned arteries were cannulated, and robot kinematics were recorded. Over-the-wire catheter exchange to a balloon catheter was performed, and balloon angioplasty was completed. The cannulations were considered successfully concluded when the angioplasty balloon was fully inflated (Fig. 2F to 2L) and the catheter and guidewire were retracted after completion of the protocol without major adverse events [21]. Finally, the animals were terminated.

Study metrics included: *(i)* success rate; *(ii)* procedure time; *(iii)* histopathology evaluation of target arteries and those traversed during the procedure for task completion. The following arteries were assessed for disruption of the intimal surface, luminal thrombus, damage to the vessel wall, and mural hemorrhage by an independent pathologist: *(i)* proximal abdominal aorta and superior mesenteric arteries; *(ii)* right and left common iliac arteries; *(iii)* abdominal aorta; *(iv)* right and left renal arteries; *(v)* aortic arch and left (base of) and right common carotid arteries.

All animal experimentation conformed to the Animal (Scientific Procedures) Act 1986 and Good Laboratory Practice Regulations 1999. All animal care, surgery, and euthanasia procedures were approved by The Griffin Institute, Northwick Park, Harrow, UK under Home Office License (Project License: XA57A4134).

A. Study Protocol

This study considered landrace crossbred pig at body weights of 60–70 kg and one-week acclimatization period prior to surgery. The choice of porcine models is based on cardiovascular anatomy comparable with human [22]. Fig. 2A to 2D show the experimental setup. The pigs showed similar vascular anatomy with absence of anomalies. The general preparation comprised commencement of anesthesia with oral administration of Diazepam (10 mg/kg) and Acepromazine (10 mg/kg). Pre-medication continued with intramuscular injection of Ketamine (5 mg/kg) and Xylazine (1 mg/kg). General anesthesia was initiated with oxygen over isoflurane and nitrous oxide face mask delivery. After endotracheal intubation, anesthesia is maintained with oxygen over isoflurane and nitrous oxide via controlled ventilation. Oxygen saturation, pulse rate, rectal temperature expired CO_2, and respiratory rate were recorded on a regular basis. An initial bolus of heparin (100 IU/kg) was administered via the arterial port followed by prophylactic boluses every 30 minutes (2000-3000 IU).

Initial vascular access to the right femoral artery was gained using a percutaneous needle (One-Part Percutaneous Entry Needle 18G 7cm, Cook Medical Europe, Limerick, Ireland), under ultrasound observation (Seldinger technique). An introducer (Radifocus II sheath, 6Fr, Terumo UK Ltd., Surrey, UK) was inserted and advanced under fluoroscopy slightly beyond the internal iliac artery to secure instrument access. Prior to each task of the study, a roadmap of the specific anatomy and landmarks was created using contrast injections delivered by an angiography catheter (Impress 5F 90 cm PIG, Merit Medical UK, Reading, UK). Afterwards, the catheter was exchanged for task specific models and soft/stiff guidewires were selected according to the procedural workflow. The list of instruments used in the in-vivo works can be found in Supplemental Table I.

In the manual scenario, the subject manipulated catheters and guidewires conventionally in proximity to the animal. In the robotic scenario, the clinician manipulated catheters and guidewires remotely using the master manipulator from a dedicated area. The operator controlled the robot exclusively based on the customized user interface and imaging data augmented by robotic status information. The robotic hardware was connected to the task-specific instrumentation with customized torque transmission components. This intraoperative assembly takes only a few seconds. The prepared unit was positioned in parallel to the right porcine femur (Fig. 2B). The optimal robot pose was set using an adjustable mounting arm attached to the rail of the floating table. If

required by the procedural workflow, an assistant exchanged instruments using the quick-exchange interfaces of the robot as shown in sequence OR1 in the Supplemental Video. In total, four tasks were provided as highlighted in Fig. 2E to 2L that targeted the following anatomy: cannulation of (*i*) LCIA via right common iliac artery, (*ii*) RRA and LRA via abdominal aorta, (*iii*) SMA via abdominal aorta, and (*iv*) RCCA via abdominal aorta and aortic arch. After robotic or manual branch cannulation, simulation of angioplasty with over-the-wire exchange and dilatation of a balloon catheter under selective digital subtraction angiography with injection of iodinated contrast agent (Encore 26 Inflator, Boston Scientific, Hemel Hempstead, UK) was performed (see sequence OR3 in the Supplemental Video). This involved application of four different devices (see instrument details in Supplemental Materials) per trial with a comparable sequence of use in all experiments including two exchanges (guidewire, catheter). Catheters and guidewires were removed with the sheath *in-situ* to prevent hemorrhage. After completion of each task series, animals were terminated under general anesthesia using sodium pentobarbitone (140 mg/kg). Sequence OR2 of the Supplemental Video demonstrates the in-vivo manipulation.

B. *Post-Mortem Tissue Assessment*

Necropsy of the animals was performed with exposure of the vascular tree within 15 minutes after termination. Target arteries and those traversed during the procedure were explanted (Fig. 5A to 5C) as follows: *Specimen 1* proximal abdominal aorta and superior mesenteric arteries; *Specimen 2* right and left iliac, abdominal aorta, right and left renal arteries; *Specimen 3* aortic arch, brachiocephalic trunk, and left (base of) and right common carotid arteries. The specimens were then fixed in formalin and sent to an independent laboratory (PathCelerate Ltd, Cheshire, UK) for histological examination. A macroscopic examination of the fixed specimens was performed to determine the appropriate tissue planes to analyze, before embedding in paraffin wax, cutting sections at approximately 5um, and staining with Hematoxylin and Eosin, with selected step-sections stained with Van Gieson and Masson's Trichrome. Resulting sections (Fig. 5) were assessed by a specialist pathologist, 'blinded' as to the method of cannulation (manual, robotic). Each section was assessed for disruption of the intimal surface, luminal thrombus, damage to the vessel wall, and mural hemorrhage. The scoring system for evaluating the sections, based on the protocol in Bismuth *et al.* [23], is summarized in Supplemental Table II.

C. *Statistics*

Data were analyzed using MATLAB (MathWorks, Inc.). Results are reported as mean ± standard deviation or %, and were compared within groups (Robotic group, and Manual group) using the Wilcoxon rank sum test. A p value <0.05 was considered to indicate statistical significance.

IV. Results: In-Vivo Validation

Results are shown in Fig. 3, 4, 5, and summarized in Tables I, II, and III.

A. *Performance Assessment*

The procedures were successful for all target vessels in both robotic (*R=2*) and manual (*M=2*) procedures (Table I). The surgeon cannulated all arteries and deployed/inflated the angioplasty balloon with a 100% success rate. Fig. 3A reports an exemplary successful robotic cannulation of the RRA, showing the temporal manipulation sequence of alternating wire and catheter manipulation to reach the target location in the artery and inflate the angioplasty balloon subsequently. Fig. 3B presents the corresponding kinematics of the remote manipulator, showing the linear and angular displacements of the catheter and guidewire drivers for each phase of the cannulation sequence. The task completion relies on successive feeding and retraction patterns of the instruments similarly to manual execution. More complex interaction of angular and linear input is presented in the supplemental video.

The average completion time was (15±6) minutes for the manual procedure, significantly lower (p = 0.03) than robotics which was (35±14) minutes (Table I, Fig. 3C). The completion time includes instruments and robot (when used) setup but does not consider the time required to anesthetize the animal and to

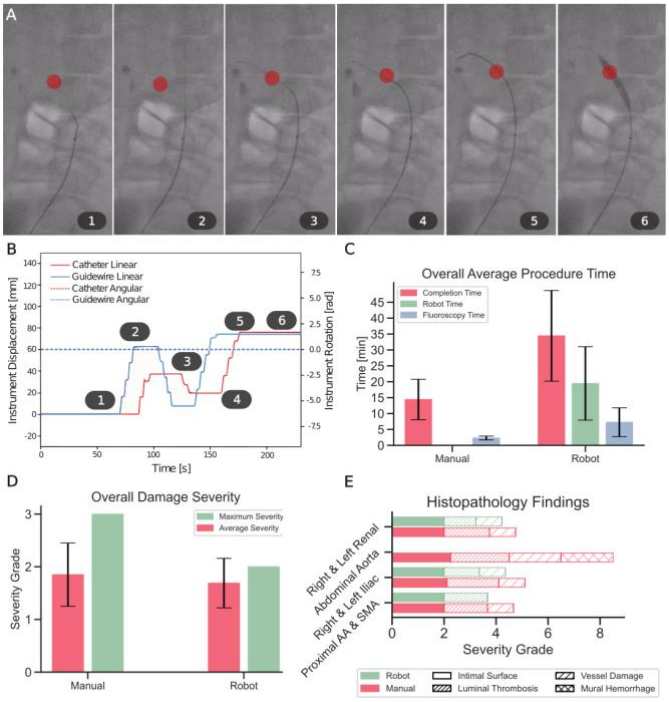

Fig. 3. Experiment results. (A) Exemplary catheter/guidewire manipulation sequence for robotic cannulation of RRA. (B) Corresponding catheter and guidewire displacements and rotations along each phase of the sequence. (C) Overall average completion time, robot time, and fluoroscopy time are reported for manual and robotics procedures. (D) Both average and maximum damage severity to vessel walls are overall lower when the robot is used. (E) Summary of histopathology findings observed in the target arteries and those traversed during the procedure: proximal abdominal aorta and superior mesenteric arteries; abdominal aorta; right and left iliac arteries; right and left renal arteries. The plots show the severity grade of structural injuries and morphological disruption in terms of observations in the intimal surface, luminal thrombosis, vessel damages, and mural hemorrhage, for manual and robotics procedures. No observations were reported in the vascular route which includes the aortic arch, brachiocephalic trunk, and left (base of) and right common carotid arteries. It is worth noting that the severity grade is zero for robotic navigation of the abdominal aorta. The severity grading is according to the scoring proposed by Bismuth *et al.* [23].

TABLE I
IN-VIVO VALIDATION: PERFORMANCE RESULTS

Target Artery	Modality	Success Rate (%)	Procedure Time [mm:ss]*		
			Completion Time	Robot Time	Fluoroscopy Time
LCIA	Manual	100	14:37 ± 04:55	-	02:17 ± 00:46
	Robotic	100	35:07 ± 02:53	18:41 ± 02:03	07:28 ± 02:25
RRA	Manual	100	12:49 ± 01:35	-	01:35 ± 00:12
	Robotic	100	22:37 ± 07:12	09:32 ± 00:28	03:39 ± 00:02
LRA	Manual	100	06:49 ± 01:25	-	01:54 ± 00:24
	Robotic	100	19:58 ± 06:40	10:48 ± 00:08	04:07 ± 00:24
SMA	Manual	100	13:47 ± 00:49	-	04:08 ± 00:15
	Robotic	100	58:12 ± 03:13	39:46 ± 07:39	16:11 ± 02:12
RCCA	Manual	100	25:30 ± 01:38	-	02:35 ± 00:10
	Robotic	100	37:47 ± 01:30	20:08 ± 07:45	05:46 ± 01:47
Average	*Manual*	*100*	***14:42 ± 06:34***	-	***02:30 ± 00:59***
	Robotic	*100*	***34:44 ± 14:26***	*19:47 ± 11:55*	***07:26 ± 04:53***

* mean ± standard deviation. Bold numbers are statistically significant with $p < 0.05$.
LCIA = left common iliac artery; RRA = right renal artery; LRA = left renal artery; SMA = superior mesenteric artery; RCCA = right common carotid artery.

TABLE II
IN-VIVO VALIDATION: KINEMATIC AND DYNAMIC ROBOT PARAMETERS

Target Artery	Catheter Platform						Guidewire Platform					
	Velocity [mm/s]*	Max. Velocity [mm/s]	Angular Velocity [rad/s]*	Max. Angular Velocity [rad/s]	Total Distance [mm]	Total Angle [rad]	Velocity [mm/s]*	Max. Velocity [mm/s]	Angular Velocity [rad/s]*	Max. Angular Velocity [rad/s]	Total Distance [mm]	Total Angle [rad]
LCIA (T1)	10.7 ± 4.8	21.0	0	0	175	0	7.8 ± 4.0	24.0	2.4 ± 1.1	6.0	355	21.7
LCIA (T2)	8.2 ± 4.2	30.0	1.8 ± 0.7	3.7	270	18.5	8.5 ± 4.1	24.0	2.1 ± 1.3	7.3	373	37.6
RRA (T1)	7.1 ± 3.2	15.0	2.0 ± 0.6	2.4	125	3.7	7.4 ± 3.1	18.0	0	0	190	0
RRA (T2)	7.8 ± 3.7	20.0	0	0	110	0	9.8 ± 4.3	21.0	0	0	230	0
LRA (T1)	8.2 ± 3.5	18.0	1.9 ± 0.9	3.7	180	4.3	7.5 ± 3.7	18.0	0	0	185	0
LRA (T2)	8.3 ± 4.0	21.0	2.0 ± 0.8	3.7	273	8.5	7.8 ± 4.4	21.0	1.2 ± 0.1	2.4	172	0.3
SMA (T1)	7.4 ± 3.8	21.0	1.7 ± 0.7	3.4	384	12.5	7.2 ± 3.6	27.0	2.3 ± 1.4	8.6	460	41.3
SMA (T2)	9.4 ± 3.3	18.0	2.0 ± 0.8	3.7	336	9.8	8.5 ± 4.0	24.0	2.0 ± 1.3	6.0	396	28.5
RCCA (T1)	10.1 ± 3.5	21.0	1.8 ± 0.6	2.4	142	2.4	6.9 ± 3.3	24.0	2.0 ± 1.2	7.3	225	5.4
RCCA (T2)	6.5 ± 3.7	15.0	1.6 ± 0.6	2.4	191	4.5	6.8 ± 3.0	18.0	1.4 ± 0.5	2.4	240	4.3

* Mean ± standard deviation of device velocities over motion sequences. Total distance and angle are cumulative results over executed linear/angular motions of each trial. T1 and T2 denote the respective in vivo trial numbers. LCIA = left common iliac artery; RRA = right renal artery; LRA = left renal artery; SMA = superior mesenteric artery; RCCA = right common carotid artery.

setup the operating room. During the robotic procedures, the robot was actually used for less than (20±12) minutes on average. The difference between the completion time and the robot time takes in account the robotic platform setup and positioning. The average fluoroscopy time during the manual procedure yielded (2±1) minutes, and (7±5) minutes when the robot was used ($p = 0.03$).

B. Robotic Platform Dynamics

These temporal observations are also reflected by recorded robot kinematics summarized in Table II. Low robot times in the RRA correspond to absence of angular guidewire motion and minor use of angular catheter input. Thus, the operator was able to cannulate the targeted vessel with less than 130 mm total catheter displacement. On the contrary, the challenging robotic cannulation of the SMA is reflected by total instrument displacements of more than 300 mm and excessive angular guidewire input of more than 28 rad. Overall, tasks were completed with mean feeding/retraction rates between 7 to 10 mm/s and mean angular rates between 1.6 to 2.0 rad/s, respectively. The maximum linear velocity of 30 mm/s (pneumatic stepper limit) was achieved in the LCIA cannulation. The maximum angular velocity of 8.6 rad/s was

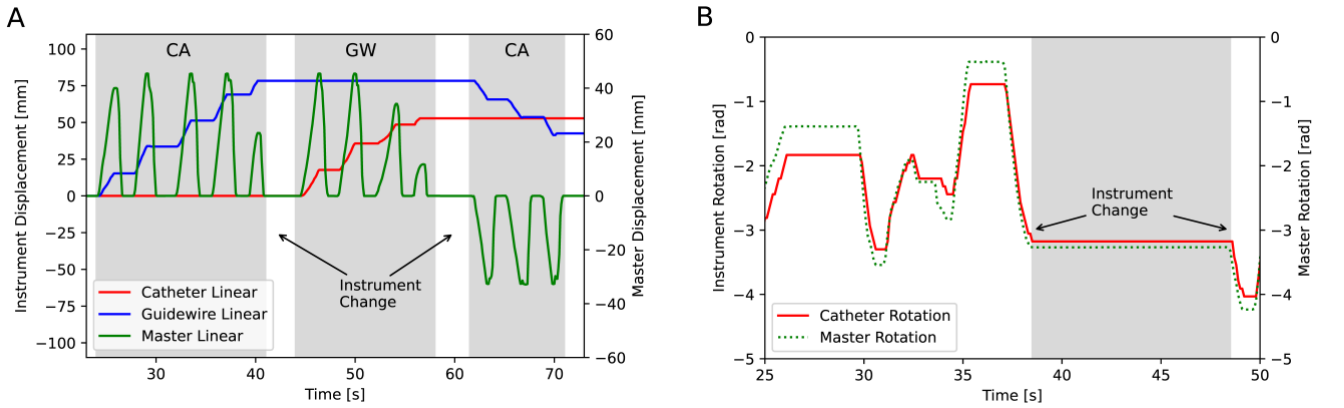

Fig. 4. Kinematic tracking performance of master and remote pneumatic manipulator. (A) Displacement of catheter and guidewire induced by repeated master input in trial LCIA T1. The latter is composed of operator input phase and the automatic homing procedure. This sequence further shows two instrument changes on the master side. (B) Angular tracking performance of master input and catheter in trial SMA T2. Residual tracking errors between master and remote manipulator reflect the current hardware limitations on angular input velocities, i.e., the desired angular dynamics.

executed in SMA cannulation. An example of linear and angular device tracking performances, according to Thakur *et al.* [24], i.e., the remote replication of executed master motions, is presented in Fig.4. In this series of in vivo experiments, the residual linear tracking error (with motion scaling factor) was 3.1±1.7 mm and the angular error yielded 0.3±0.1 rad. The corresponding delay between master command and response of the remote manipulator yielded to 108±12 ms.

C. *Histopathology Results*

The histopathology results (Table III, Fig. 3D, 3E, Fig. 5) showed that, in general, structural injury, and resultant morphologic/architectural disruption, was relatively minor with both robotic and manual endovascular techniques. There were group differences, notably with regard to the incidence and/or severity of change, and also the presence of subendothelial vessel damage. The average number of sections with observations was lower when the robot was used with respect to manual resulting in 33 and 47 observations respectively (p = 0.57). Both average and maximum severity of such observations was higher in manual procedures over robotics, although with no statistical significance ($p > 0.05$ in both cases). However, there was a significantly (p = 0.04) lower number of sites with vessel damages when the robot was used (2 sites) over manual (21 sites).

The *proximal abdominal aorta and the superior mesenteric arteries* (Fig 3E, Fig. 5A, 5A1, 5A2, 5B1, 5B2) were relatively quiescent in terms of structural change. Robotic intervention led to near absence of histopathologic findings. Of the 18 sections examined only 6 presented minor observations with a small number of relatively minor endothelial and thrombotic observations in only one animal. However, common to both animals was a lack of underlying vessel damage. Both animals which received manual operation presented 14 sections with minor endothelial and thrombotic observations, and vessel

TABLE III
IN-VIVO VALIDATION: HISTOPATHOLOGY RESULTS

Specimen	**Modality**	**Sections**			**Severity**	
		Evaluated	With Observations	With Damages	Mean*	Max
PA, SMA	Manual	18	14	3	1.80 ± 0.40	2
	Robotic	18	6	0	1.80 ± 0.40	2
CIAs	Manual	18	18	8	1.76 ± 0.78	3
	Robotic	18	13	2	1.64 ± 0.48	2
AA	Manual	6	4	3	2.18 ± 0.57	3
	Robotic	6	0	0	0	0
RAs	Manual	18	11	7	1.65 ± 0.48	2
	Robotic	18	14	0	1.64 ± 0.48	2
Ao.Arch, CCAs	Manual	18	0	0	0	0
	Robotic	18	0	0	0	0
Overall	*Manual*	*78*	*47*	***21***	*1.85 ± 0.60*	*3*
	Robotic	*78*	*33*	***2***	*1.69 ± 0.47*	*2*

* mean ± standard deviation. Bold numbers are statistically significant with $p < 0.05$.
PA = proximal abdominal aorta; SMA = superior mesenteric artery; CIAs = common iliac arteries; AA = abdominal aorta; RAs = renal arteries; Ao.Arch = aortic arch; CCAs = common carotid arteries.

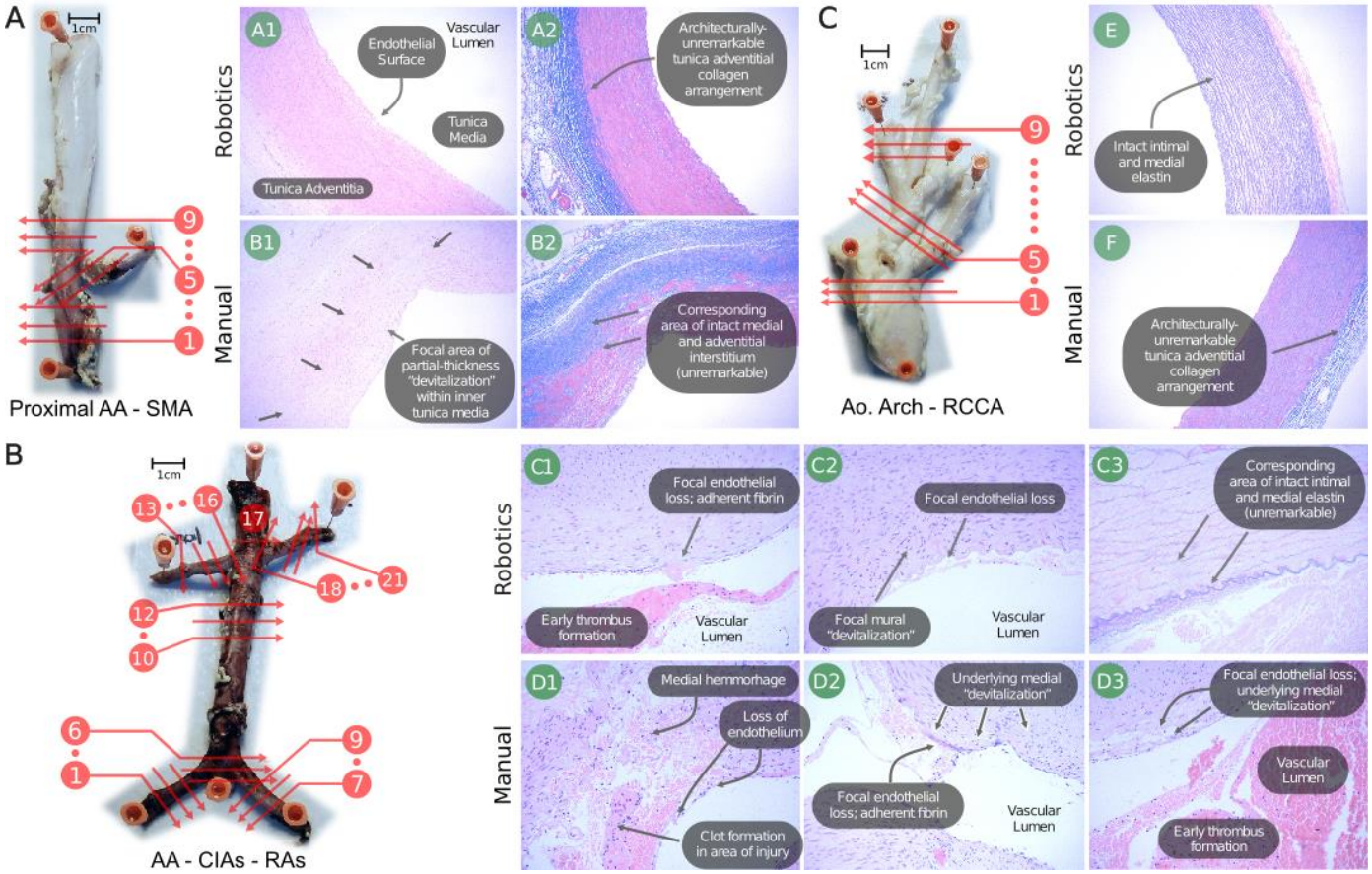

Fig. 5. Exemplary specimens and histopathology findings for robotics and manual interventions. Specimens explanted post-mortem for histological examination. Target arteries and those traversed during the procedure were explanted and assessed along selected cutting sections (see section labelling of each subfigure). (A) Specimen 1: proximal abdominal aorta and superior mesenteric arteries (9 sections). (B) Specimen 2: right and left iliac arteries (9 sections); abdominal aorta (3 sections); right and left renal arteries (9 sections). (C) Specimen 3: aortic arch, brachiocephalic trunk, and left (base of) and right common carotid arteries (9 sections).

Histopathology findings: (A1, A2) Aorta/Superior Mesenteric Artery Junction, Section 5, 5x objective (Robotics): note the normal architecture. (B1, B2) Aorta/Superior Mesenteric Artery Junction, Section 5, 5x objective (Manual) presence of devitalization in the inner tunica media (B1) and intact medial and adventitial interstitium (B2). (C1) Iliac Artery Junction, Section 5, 20x objective (Robotics): presence of focal endotheliosis loss, adherent fibrin, and early thrombus formation. (C2) Iliac Artery Junction, Section 5, 20x objective (Robotics): focal mural devitalization and endothelial loss. (C3) Iliac Artery Junction, Section 5, 20x objective (Robotics): corresponding area of intact intimal and medial elastin. (D1) Abdominal Aorta, Section 10, 20x objective (Manual): presence of transmural disruption with medial hemorrhage and clot formation in the area of the injury. (D2) Right Renal Artery, Section 14, 20x objective (Manual): underlying medial devitalization and endothelial loss with adherent fibrine. (D3) Iliac Artery Junction, Section 5, 20x objective (Manual): focal endothelial loss with underlying medial devitalization and early thrombus formation. (E) Brachiocephalic Trunk, Section 5, 5x objective (Robotics): normal architecture. (F) Brachiocephalic Trunk, Section 5, 5x objective (Manual): normal architecture.

damage at 3 sites (focal devitalization of the tunica).

Pathologic findings were more pronounced in the arterial bed of the *abdominal aorta, common iliac, and renal arteries* (Fig. 3E, Fig. 5B, Fig. 5C1 to 5C3, Fig. 5D1 to 5D3). This is consistent with a greater degree of intervention/manipulation within associated vascular profiles. These intervention sites were generally characterized, amongst robotically endocatheterized animals, by minimal-to-mild endothelial and thrombotic structural findings, with rare findings of minimal "devitalization" of the underling tunica muscularis, observed in only two sites of the common iliac arteries of one animal. No damages and hemorrhage were reported in the abdominal aorta and renal arteries of both animals. In manually endocatheterized animals, there was generally a higher incidence and/or severity of endothelial/thrombotic findings, and these observations were associated with a higher incidence (18 sites in total, 8 in the CIAs, 3 in the abdominal aorta, and 7 in the RAs) of vascular "devitalization", and with sporadic and isolated findings of medial hemorrhage, elastin fragmentation/splitting, and structural collagen distortion.

Finally, the vascular route which includes the *aortic arch, brachiocephalic trunk, and left and right common carotid arteries* (Fig. 5C, 5E, 5F), was devoid of structural pathology, in all animals, for both robotic and manual intervention.

V. Discussion

This study was designed to complement the benchtop assessment of the robotic platform conducted in [19] (the cannulation tasks were the same), and to provide clinically relevant outcome data. Building on the findings of the benchtop validation, including usability feedback from 7 expert vascular surgeons on the robotic system, the platform was refined in preparation of the in-vivo assessment here presented.

The results reported in this study, showed that the robot

success rate was 100% in all cannulation tasks (Table I). The surgeon easily navigated the vasculature and successfully positioned and inflated the balloon angioplasty in the selected target arteries (see Fig. 3A, and 3B as an example), demonstrating the feasibility of our robot. The success rate in manual cannulation was 100% in all cases.

The analysis of surgery times (Table I, Fig. 3C) showed that robotic procedures could be completed in about 35 minutes, including robot setup (about 15 minutes), and the actual robotic manipulation of less than 20 minutes (average values). Manual procedures could be completed in about 15 minutes. The comparison of robot time and manual completion time shows that the actual robotic manipulation was only 5 minutes longer than the manual on average, which corresponded to 5 minutes longer fluoroscopy time (about 2 minutes in manual cases, 7 minutes in robotic cases). Both setup and robotic time can be further reduced by optimizing the design of the remote manipulator and its positioning device (Fig. 2D). Robot positioning requires to undo the joint screws of the arm, move the robot to the desired pose and tighten the screws back (time consuming). A bespoke mechanism should be developed for a quicker positioning of the remote manipulator. The restricted dynamics of the remote manipulator caused by the inherent delay (~100 ms) of pneumatic power transmission and hardware design limitations did not allow a quick manipulation of the instruments, in particular their translation. This is also reflected by the linear and angular tracking performances which are to date dynamically and technologically inferior to, e.g., MR-compatible piezo actuated mechanisms in [24]. An improved pneumatic design of the linear actuators can potentially improve the speed of the system beyond 30 mm/s and achieve better dynamic performances, both for linear and angular displacement. It is worth highlighting that the quick-exchange interface of the remote manipulator (Fig. 1F) allowed the surgeon's assistant to seamlessly exchange the instruments (i.e., catheters and guidewires) without time consuming handling of the robotic hardware (Fig. 2B, 2C). We believe this is a notable achievement in terms of clinical usability and integration within the surgical workflow.

Although these data confirm that the robot slightly extends the procedure time – while remaining in an acceptable range for clinical use – they also demonstrate the increased safety for the operator when the procedure is carried on robotically. The robot is teleoperated from the control room, where the surgeon is shielded from x-ray exposure. This is a major advantage in terms of safety, as it is well documented that prolonged exposure to x-rays may cause life threatening damages to surgeons [25]. In terms of patient safety, a slightly longer procedure and fluoroscopy time can be justified by a potentially safer robotic procedure, with lower occurrence and severity of injuries.

The histopathology results (Table III, Fig. 3D, 3E, Fig. 5) support this assumption, showing that structural injuries and morphologic/architectural disruption were relatively minor when the robot was used, especially with regard to the incidence and/or severity of change, and also the presence of subendothelial vessel damage. Of the 78 sections examined for each modality (robotic, manual) only 42% reported minor observations when the robot was used against 60% for the manual procedures. The robotic procedures resulted in only 2 sections with vessel damages in the CIAs with low severity. No vessel damage was reported elsewhere. On the contrary, manual procedures showed a total of 21 sections with vessel damages of higher grade in every specimen, with the only exclusion of the aortic arch and common carotid arteries, where the relatively large diameter and linear vascular profile resulted in lower mechanical contact trauma. Such damages were particularly notable within regions of the abdominal aorta, iliac, and renal arteries, wherein animals subject to manual endocatheterization also had additional morphologic findings, i.e., a greater spectrum of structural change. Due to its stability and guidance, the robot allowed the surgeon to navigate the vessels with a higher level of accuracy, thus reducing the damage it causes, as demonstrated by the less significant grade of injuries in the robotic cases versus the manual control. These findings are in agreement with the results obtained in the benchtop trials (please refer to [19]) where our robot resulted in lower manipulation forces applied to the vasculature with respect to manual, i.e., potentially resulting in lower vessel damages. Also, manipulation forces measured with our platform in [19] were in line with data reported in literature [26], further providing confidence in favor of its clinical applicability.

VI. Open Challenges and Future Directions

In terms of study design, limitations are the relatively low number of experimental trials with a narrow scope of manipulation tasks. Also, having the same clinician to perform both manual a robotic navigation (i.e., the operator cannot be blinded to the method of use) is another major limitation. The analysis of dynamics (i.e., velocities, accelerations) of the vascular instruments during the different navigation modalities would help to address such limitation, and better understand the causes of difference in vascular damage. Future developments and experiments will aim at improving such limitations.

Although this study (and others reported in literature, e.g., [23]) indicates that vessel wall damage can be reduced using a robot in conjunction with standard 2D fluoroscopy, a major open challenge remains the exploitation of 3D imaging. Imaging in this study was in a 2D (anteroposterior) plane, thus limiting the image-guided haptic guidance to the imaging plane, i.e., the catheter/vessel contacts out of the imaging plane - or normal to the imaging plane - are not detected. This clearly represents a major limitation of the current platform. While in the case of vessels with large lumen (as in this study) such 2D guidance has yet a positive impact on the procedure, 3D imaging should be employed to achieve optimal guidance. In preliminary work [17] we have demonstrated that integrating 3D imaging (3D fluoroscopy) to our robotic platform (although in a simulated environment) has the potential of improving effectiveness, precision, and safety of endovascular procedures. However, transition from simulation to real application in a clinical environment still remains difficult. Main limitations include quick and reliable registration between pre- and intra-operative images, which requires a real-time recovery of

vascular motion and deformation caused by the cardio-respiratory motion [27]. We also envision that in the future MRI may be incorporated to the procedural workflow to improve diagnosis, planning, navigation, and execution of endovascular interventions, by providing 3D functional and radiation-free imaging, enhanced visualization of soft tissues, and even characterization of the blood flow. To this regard, we believe that the reporting of our system, and in particular the MR-safe technology of our robot will encourage comprehensive research and development towards this evolution. Opportunities lie in the development of real-time MR image sequences and processing, and development of MR-safe devices such as steerable catheters, with potential application to pediatrics [28]. Another open challenge for endovascular robotics is the development of platforms with increased level of autonomy and cooperation with the clinical team. For example, future endovascular robots should be able to perform autonomously a set of routine procedures (e.g., navigating a wire through the vasculature to reach the point of treatment) and leave complete control to the users, or cooperate with them, during critical steps (e.g., positioning of a stent). Shared-control, by increasing the level of autonomy of robotic platforms and enhancing the cooperation with vascular surgeons, will be a first step towards the transition to fully autonomous execution of endovascular procedure, as our preliminary work [29], [30] on integrating AI into endovascular robotics suggests. However, more research needs to be conducted in the future by both industry and academia in order to address these challenges, not only in the area of endovascular intervention, but more in general of medical robotics [31].

VII. Conclusion

This study demonstrates the feasibility and safety of our robotic platform on porcine models, paving the way for clinical translation. Data confirms that it can resolve challenges of precise endovascular navigation, surgical workflow integration, and safety, as demonstrated by successful in-vivo trials.

References

[1] J. Troccaz *et al.*, "Frontiers of Medical Robotics: From Concept to Systems to Clinical Translation," *Annual Review of Biomedical Engineering*, vol. 21, no. 1, pp. 193–218, 2019.

[2] J. A. Smith *et al.*, "30 Years of Neurosurgical Robots: Review and Trends for Manipulators and Associated Navigational Systems," *Ann Biomed Eng*, vol. 44, no. 4, pp. 836–846, Apr. 2016.

[3] G. Dagnino *et al.*, "Image-Guided Surgical Robotic System for Percutaneous Reduction of Joint Fractures," *Ann Biomed Eng*, vol. 45, no. 11, pp. 2648–2662, Nov. 2017.

[4] G. Dagnino *et al.*, "Design and Real-Time Control of a Robotic System for Fracture Manipulation," IEEE EMBC, Milan, Italy, 2015.

[5] D. Kundrat *et al.*, "Preclinical Performance Evaluation of a Robotic Endoscope for Non-Contact Laser Surgery," *Ann Biomed Eng*, vol. 49, no. 2, pp. 585–600, Feb. 2021.

[6] G. Dagnino *et al.*, "A vision-based system for fast and accurate laser scanning in robot-assisted phonomicrosurgery," *Int J Comput Assist Radiol Surg*, vol. 10, no. 2, Art. no. 2, 2015.

[7] J. W. Yaxley *et al.*, "Robot-assisted laparoscopic prostatectomy versus open radical retropubic prostatectomy: early outcomes from a randomised controlled phase 3 study," *The Lancet*, vol. 388, no. 10049, pp. 1057–1066, Sep. 2016.

[8] R. Estape, "Early Acute In-vivo Experience in Gynecology Oncology Applications with the SPORT Surgical System Technology," 2018.

[9] H. Rafii-Tari *et al.*, "Current and emerging robot-assisted endovascular catheterization technologies: a review," *Annals of Biomedical Engineering*, vol. 42, no. 4, pp. 697–715, Apr. 2014.

[10] S.-L. Lee *et al.*, "Devices for Endovascular Interventions: technical advances and translational challenges," White paper, 2017.

[11] T. G. Walker *et al.*, "Clinical practice guidelines for endovascular abdominal aortic aneurysm repair", *Journal of vascular and interventional radiology*, vol. 21, no. 11, pp. 1632–1655, 2010.

[12] Shi Rui *et al.*, "Epicardial Ventricular Tachycardia Ablation Guided by a Novel High-Resolution Contact Mapping System: A Multicenter Study," *Journal of the American Heart Association*, vol. 7, no. 21, p. e010549, Nov. 2018.

[13] C. Molvar and R. J. Lewandowski, "Intra-Arterial Therapies for Liver Masses: Data Distilled," *Radiol. Clin. North Am.*, vol. 53, no. 5, pp. 973–984, Sep. 2015.

[14] P. F. Ludman, "UK TAVI registry," *Heart*, vol. 105, no. Suppl 2, pp. s2–s5, Mar. 2019.

[15] G. Dagnino *et al.*, "Haptic Feedback and Dynamic Active Constraints for Robot-Assisted Endovascular Catheterization," IEEE/RSJ International Conference on Intelligent Robots and Systems (IROS), Madrid, Spain, 2018.

[16] M. Abdelaziz *et al.*, "Toward a Versatile Robotic Platform for Fluoroscopy and MRI-Guided Endovascular Interventions: A Pre-Clinical Study," IEEE/RSJ International Conference on Intelligent Robots and Systems (IROS), Macau, 2019.

[17] M. Benavente Molinero *et al.*, "Haptic Guidance for Robot-Assisted Endovascular Procedures: Implementation and Evaluation on Surgical Simulator," IEEE/RSJ International Conference on Intelligent Robots and Systems (IROS), Macau, 2019

[18] C. J. Payne *et al.*, "A force feedback system for endovascular catheterisation," in *2012 IEEE/RSJ International Conference on Intelligent Robots and Systems*, Oct. 2012, pp. 1298–1304.

[19] D. Kundrat *et al.*, "An MR-Safe Endovascular Robotic Platform: Design, Control, and Ex-Vivo Evaluation," *IEEE Transactions on Biomedical Engineering*, pp. 1–1, 2021.

[20] G. Dagnino *et al.*, "Haptic Feedback and Dynamic Active Constraints for Robot-Assisted Endovascular Catheterization," IEEE/RSJ International Conference on Intelligent Robots and Systems (IROS), Madrid, Spain, 2018.

[21] J. F. Granada *et al.*, "First-in-human evaluation of a novel robotic-assisted coronary angioplasty system," *JACC Cardiovasc Interv*, vol. 4, no. 4, pp. 460–465, Apr. 2011.

[22] M. M. Swindle *et al.*, "Swine as models in biomedical research and toxicology testing," *Vet Pathol*, vol. 49, no. 2, pp. 344–356, Mar 2012.

[23] J. Bismuth *et al.*, "Feasibility and safety of remote endovascular catheter navigation in a porcine model," *J Endovasc Ther*, vol. 18, no. 2, Art. no. 2, Apr. 2011.

[24] Y. Thakur *et al.*, "Characterization of catheter dynamics during percutaneous transluminal catheter procedures," *IEEE Trans Biomed Eng*, vol. 56, no. 8, pp. 2140–2143, Aug. 2009.

[25] M. L. Kirkwood *et al.*, "Surgeon radiation dose during complex endovascular procedures," *J Vasc Surg*, vol. 62, no. 2, pp. 457–463, Aug. 2015.

[26] H. Rafii-Tari *et al.*, "Objective Assessment of Endovascular Navigation Skills with Force Sensing," *Ann Biomed Eng*, vol. 45, no. 5, pp. 1315–1327, May 2017.

[27] S.-L. Lee *et al.*, "Motion-adapted catheter navigation with real-time instantiation and improved visualisation," *J Robot Surg*, vol. 7, no. 3, Art. no. 3, Sep. 2013.

[28] A. Massmann *et al.*, "Glass-Fiber-based MR-safe Guidewire for MR Imaging-guided Endovascular Interventions: In Vitro and Preclinical in Vivo Feasibility Study," *Radiology*, vol. 284, no. 2, pp. 541–551, Aug. 2017.

[29] W. Chi *et al.*, "Trajectory Optimization of Robot-Assisted Endovascular Catheterization with Reinforcement Learning," p IEEE/RSJ International Conference on Intelligent Robots and Systems (IROS), Madrid, Spain, 2018.

[30] W. Chi *et al.*, "Collaborative Robot-Assisted Endovascular Catheterization with Generative Adversarial Imitation Learning," IEEE Int. Conf. Robotics and Automation (ICRA) Paris, 2020.

[31] G.-Z. Yang *et al.*, "The grand challenges of Science Robotics," *Science Robotics*, vol. 3, no. 14, p. eaar7650, Jan. 2018.